

Harnessing *Sterculia foetida* Seed Coat for Silver Nanoparticles Biofabrication: Characterization and A Rapid, Highly Efficient Catalyst for Methylene Blue Degradation

Oman Zuas^{1,*} , Fakhzah Aliifatudz Dzakhirah² , Toto Sudiro³ 

¹ Research Center for Testing Technology and Standards, National Research and Innovation Agency (BRIN), K.S.T-BJ. Habibie, Building 417, South Tangerang 15314, Indonesia

² Chemistry Department, Faculty of Natural Science, Universitas Negeri Malang, Semarang Street No.5, 65145, East Java, Indonesia

³ Research Center for Advanced Materials, National Research and Innovation Agency (BRIN), K.S.T-BJ. Habibie, Building 420-422, South Tangerang 15314, Indonesia

* Correspondence: oman003@brin.go.id;

Received: 16.03.2025; Accepted: 11.05.2025; Published: 8.06.2025

Abstract: Our study presents an environmentally friendly method for fabricating silver nanoparticles (Ag-NPs) by applying the water extract of the *Sterculia foetida* (SFSC) seed coat as both a reducing and stabilizing agent. We also examined their effectiveness in catalyzing methylene blue (MB) degradation. The successful fabrication of SFSC-Ag-NPs was confirmed through various analyses, including UV-Vis spectroscopy, Dynamic Light Scattering (DLS), Fourier Transform Infrared Spectroscopy (FTIR), X-ray Diffraction (XRD), and Transmission Electron Microscopy (TEM). A peak in surface plasmon resonance indicated the development of colloidal SFSC-Ag-NPs at 432 nm within the UV-Vis absorbance spectrum. The SFSC-Ag-NPs demonstrated good stability, evidenced by a negative zeta potential of -63.8 mV. XRD diffractograms revealed that the crystal structure of SFSC-Ag-NPs is a face-centered cubic with creditable crystalline properties. HR-TEM results revealed that the SFSC-Ag-NPs exhibit quasi-spherical and hexagonal shapes, averaging 14.42 nm in size. The results of the catalytic performance indicated that SFSC-Ag-NPs were highly effective in degrading MB at neutral pH, achieving a remarkable efficiency of 99.84% in just 17 minutes. The degradation process follows pseudo-1st-order kinetics, with a 9.47×10^{-2} minutes⁻¹ of rate constant. These results suggest that SFSC-Ag-NPs hold great potential for removing textile dyes in a sustainable environmental application.

Keywords: plant extract; biosynthesis; Ag-NPs; metallic nanoparticles; catalyst; dye; kinetic.

© 2025 by the authors. This article is an open-access article distributed under the terms and conditions of the Creative Commons Attribution (CC BY) license (<https://creativecommons.org/licenses/by/4.0/>), which permits unrestricted use, distribution, and reproduction in any medium, provided the original work is properly cited. The authors retain the copyright of their work, and no permission is required from the authors or the publisher to reuse or distribute this article as long as proper attribution is given to the original source.

1. Introduction

The potential health and environmental impacts associated with traditional methods of nanoparticle fabrication have sparked growing concerns. As a result, there is a heightened focus on advancing sustainable and eco-friendly approaches for nanoparticle synthesis [1, 2]. Silver nanoparticles (Ag-NPs), with exceptional physicochemical properties and potential for wide application [3-7], have attracted much attention among the various nanoparticles.

Conventionally, Ag-NPs are made utilizing chemical-reducing substances such as sodium borohydride (NaBH₄) [8, 9] and hydrazine [10, 11], which are toxic, difficult to decompose naturally and harmful to the environment.

In recent decades, the biofabrication of Ag-NPs using plant extracts has gained attention as a promising alternative method. This approach offers several advantages, including cost-effectiveness, straightforward procedures, and the abundant availability of natural resources [12-14]. The bioactive compounds in plant extracts, such as phenolics, flavonoids, alkaloids, terpenoids, and amino acids, play a crucial function in reducing and stabilizing agents during biofabrication [15]. For instance, the leaf extract of *Azadirachta indica*, known for its rich content of bioactive compounds, has been exploited in the biofabrication of Ag-NPs. These compounds help reduce silver ions (Ag⁺) to metallic silver (Ag⁰) while also stabilizing the resulting nanoparticles [16, 17]. Similarly, *Moringa oleifera* leaf extract, rich in bioactive constituents, has been utilized as a reducing and stabilizing agent in producing Ag-NPs, demonstrating notable antimicrobial properties [18, 19]. Another notable example is *Camellia sinensis* extract, which contains polyphenols that act as potent reducing agents in fabricating Ag-NPs, which have antibacterial ability and activity in degrading dyes [20].

Sterculia foetida is another essential species in the biofabrication of Ag-NPs [21, 22] known by various names such as Javanese almond, Kelumpang, Anacaguita, Telembu, and Sam Ran [23, 24]. *S. foetida*, as a tropical plant, is distributed in Asia, Africa, and Australia [24]. Aqueous extracts derived from the seeds, bark, or leaves of *S. foetida* are reported to contain bioactive molecules such as alkaloids, flavonoids, tannins, phenols, saponins, steroids, and terpenoids [25-28]. These bioactive constituents have been shown to play a vital role in the biofabrication of Ag-NPs, acting as reducing agents and at the same time as stabilizers to prevent particles from aggregating [22, 29, 30]. Biofabricated Ag-NPs from *S. foetida* have been shown to have significant activity as an antimicrobial, antioxidant, anti-cancer, and anti-inflammatory [21, 22, 29-31].

Organic dyes, widely used in various industries, pose significant ecological and health risks when disposed of in the environment [32] due to their complex chemical structure and resistance to degradation [33]. Among the organic dyes, MB is particularly well-known for its wide applications in textiles, paper, biology, medical diagnostics, and even photodynamic therapy for cancer treatment [33-35]. Nevertheless, improper discharge into water bodies can lead to environmental and adverse health consequences. Methylene blue can be toxic to aquatic life, reduce light penetration that can interfere with photosynthesis, and cause harmful effects on humans, such as skin irritation, respiratory problems, and neurotoxicity [33, 35]. Various methods for removing MB from aqueous solutions have been developed [33, 35], including advanced oxidation processes, adsorption, photocatalytic degradation, membrane filtration, and biological treatment utilizing specific microorganisms. In addition, the efficient removal of MB from the solution is also carried out by catalytic reduction using metal catalysts such as silver (Ag) [36], gold (Au) [32], and palladium (Pd) nanoparticles [37]. These metal nanoparticle catalysts accelerate the electron transfer process and facilitate the rapid breakdown of MB into less harmful compounds.

In this study, the potential of bioactive compounds in *S. foetida* seed coat water extract was evaluated as reducing and stabilizing agents in the fabrication of Ag-NPs and their use as a catalyst in degrading the carcinogenic dye MB, serving as a model compound. We hypothesize that using *S. foetida* seed coat water extract may facilitate the formation of Ag-NPs, which have unique physicochemical properties that serve as an effective catalyst for MB

degradation in aqueous solutions. The findings of this study are expected to complement previous research in similar fields in understanding the characteristics of Ag-NPs that are biofabricated using plant extracts, especially the *S. foetida* plant, which may contribute to understanding their potential role in eliminating dye from water that has not been previously reported.

2. Materials and Methods

2.1. Materials.

The following analytic grade chemicals were utilized without special treatment, including silver nitrate (analytical grade, Supelco®), methylene blue (C₁₆H₁₈ClN₃S, Supelco®), and sodium borohydride (Sigma-Aldrich®). *S. foetida* seeds (Figure 1a) were purchased from the UKI BIBIT Shop, West Java, Indonesia. Double-deionized (DD) water was utilized in all experiment runs.

2.2. Preparation of *S. foetida* water extract.

A water extract from the seed coat of *S. foetida* (marked as SFSC) was prepared using the hydrothermal method by adopting the previous procedure [38], with a slight modification. Initially, the SFSC (Figure 1b) was thoroughly cleaned to remove dirt and dust; then, it was incubated at 60°C to remove moisture content. The extraction was performed by adding 9 g of dry SFSC pieces into a Teflon-coated stainless-steel autoclave containing 45 mL of DD water. A hydrothermal treatment was conducted at 120°C for 1 hour to enhance the extraction of phytochemical compounds. Following the hydrothermal process, the autoclave with the extract solution was allowed to cool to room temperature, and the supernatant was collected by filtering through the Whatman No. 42 filter paper. The resulting brown filtrate from the SFSC water extract (referred to as SFSC water extract, as illustrated in Figure 1c, was then kept at 4°C for future use in the biofabrication of Ag-NPs.

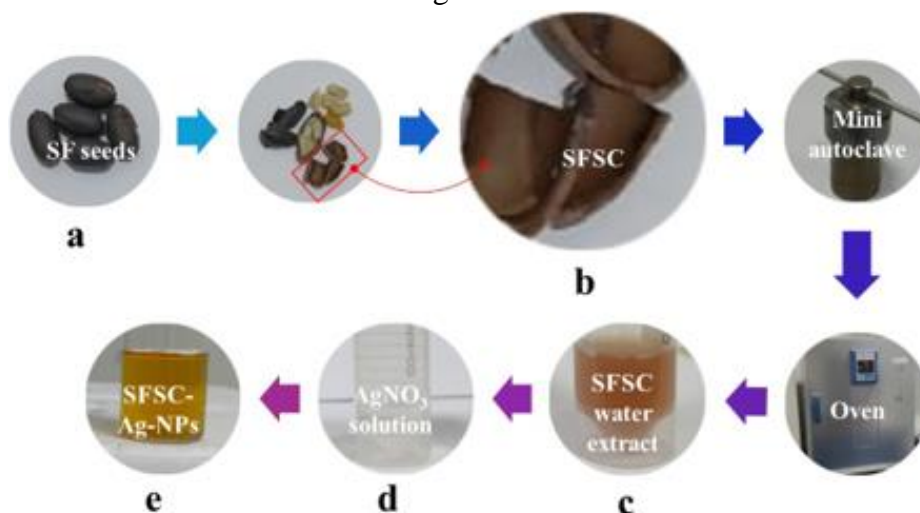


Figure 1. A diagrammatic representation of the SFSC-Ag-NPs biofabrication process: (a) seeds of *S. foetida*; (b) *S. foetida* seed coat (SFSC); (c) SFSC water extract; (d) AgNO₃ solution; (e) colloidal SFSC-Ag-NPs

2.3. Biofabrication of Ag-NPs.

Biofabrication of Ag-NPs using SFSC water extract (labeled as SFSC-Ag-NPs) was carried out as follows. The SFSC aqueous extract (500µL) was added gradually to 20 mL of

0.125 mM AgNO₃ solution and incubated at room temperature for 14 hours. Over time, there was a change in the color of the solution from a colorless AgNO₃ solution (Figure 1d) to a brownish-yellowish colloidal SFSC-Ag-NPs (Figure 1e). The color of the solution before and after the reduction process was measured using a UV-Vis spectrophotometer, and the results were compared.

2.4. Characterizations.

The following instruments were utilized to characterize the SFSC-Ag-NPs. The color change of SFSC-Ag-NPs during the biofabrication process was measured using a UV-Vis spectrophotometer (Genesys 150 ThermoFisher). The hydrodynamic diameter and zeta potential (ZP) of SFSC-Ag-NPs were recorded using Dynamic Light Scattering (DLS, SZ-100 Horiba). The presence of functional groups in the biomolecules from the SFSC water extract and the biofabricated SFSC-Ag-NPs were examined using Fourier Transform Infrared Spectroscopy (FTIR, Invenio Bruker). The crystalline properties of the SFSC-Ag-NPs were determined using X-ray diffraction (XRD, Rigaku Smartlab). A high-resolution-TEM (HR-TEM, Tecnai G2 20 S-TWIN) was employed to visually analyze the shape, size, and morphology of the SFSC-Ag-NPs.

2.5. Assessment of the catalytic performance of SFSC-Ag-NPs in MB degradation.

The catalytic performance of SFSC-Ag-NPs in facilitating the elimination of MB from the aqueous solution was investigated at neutral pH. The neutral pH refers to the findings reported by Ogundare et al. [36]. They found that MB degradation best occurred at a neutral pH of 7.5, where an 82% degradation efficiency was obtained in just 5 minutes. In contrast, at low pH 3, there was a decrease in efficiency to 44% over 16 minutes, which is thought to be an excess of protons at low pH that inhibits the interaction between cationic dyes and Ag-NPs. Meanwhile, at pH 10, the degradation efficiency only reaches 81% within 8 minutes, which is suspected to increase in negative charge of the catalyst surface due to the presence of hydroxide ions (OH⁻), which limits the interaction between the catalyst and the borohydride reducing agent (BH₄⁻). In our study, a catalytic study was performed by analyzing the effects of reaction time, initial MB concentration, and SFSC-Ag-NPs volume on MB degradation efficiency (%D) using Eq. 1 [39]. Degradation efficiency is evaluated by comparing the starting concentration with the residual MB concentration, providing insight into the effectiveness of the removal process. Additionally, the kinetics of the MB catalytic degradation reaction were assessed using 1st-order (Eq. 2) and 2nd-order kinetics (Eq. 3) [40, 41].

$$\% D = (C_0 - C_t) / C_0 \times 100 \quad (1)$$

$$\ln(C_t / C_0) = \ln(A_t / A_0) = -k_1 t \quad (2)$$

$$1 / C_t = 1 / C_0 + k_2 t \quad (3)$$

where C₀ and C_t are the initial and remaining MB (mg/L) concentrations at any time. k₁ and k₂ are the 1st-order and the 2nd-order rate constant, respectively. Meanwhile, t is the reaction time (minutes), A₀ is the absorbance at the wavelength of 664 nm, which is related to C₀, and A_t is the absorbance associated with C_t.

3. Results and Discussion

3.1. Characterizations.

UV-Vis spectroscopy is a common technique for monitoring the formation of Ag-NPs during biofabrication. Figure 2 shows the UV-vis spectrum of AgNO₃ solution, SFSC water extract, and colloidal SFSC-Ag-NPs after 12 hours of incubation. As can be seen, the spectrum of colloidal SFSC-Ag-NPs (Figure 2c) differs significantly compared to the spectrum of AgNO₃ solution (Figure 2a) and SFSC water extract (Figure 2b). Meanwhile, the colloidal SFSC-Ag-NPs showed prominent absorption between 340–520 nm, with a peak of surface plasmon resonance (SPR) at 432 nm, proving the formation of Ag⁰. However, the AgNO₃ solution containing Ag⁺ (Figure 2a) does not show significant peak absorption in this wavelength range, as Ag⁺ ions do not produce SPR features. The same is seen for the spectrum of the SFSC water extract (Figure 2b). Interestingly, the SFSC water extract showed a peak of around 280 nm. This peak is thought to take place since the biomolecules in the extract absorb light with sufficient energy, according to the transition $\pi \rightarrow \pi^*$, to promote electrons from the bonding (π) to antibonding (π^*) orbital [42].

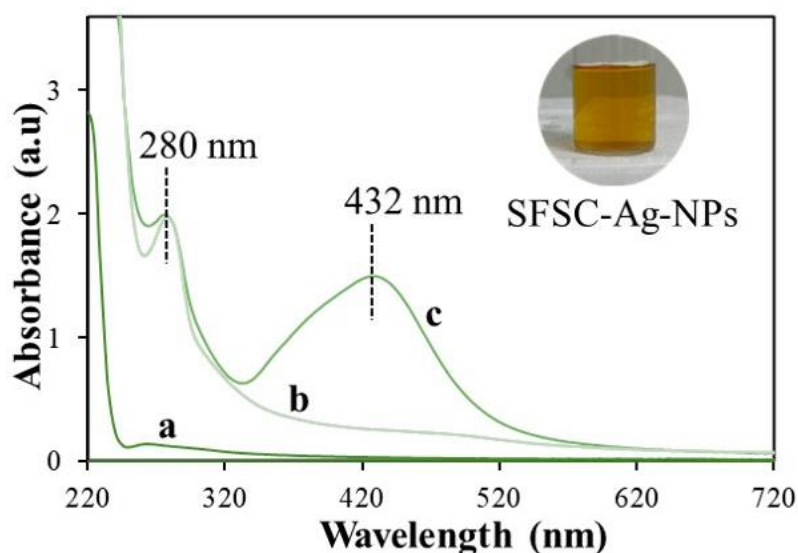


Figure 2. UV–visible spectra of (a) AgNO₃ solution; (b) SFSC water extract; (c) colloidal SFSC-Ag-NPs (solution image of colloidal SFSC-Ag-NPs; inset).

The results of these UV-Vis measurements are in line with visual data, confirming the success of fabricating SFSC-Ag-NPs. The observed data, especially the maximum peak of SPR found in this study, are close to the values reported by some previous studies [19, 38]. The characteristics of biofabricated Ag-NPs using *M. oleifera* leaf extract showed an SPR at wavelengths between 450–550 nm, with the highest peak at 477 nm [19]. Likewise, Ag-NPs synthesized using the aqueous extract of *Diospyros celebica* possessed an SPR with the highest peak at 440 nm and a smaller peak at 356 nm, presumably due to the electronic transition of the capping biomolecule [38].

Dynamic Light Scattering (DLS) is a widely used technique for assessing the particle size distribution and zeta potential (ZP) of nanoparticles in suspension [43]. The measurements of colloidal SFSC-Ag-NPs revealed an average particle size (z-average) of 53.3 nm (Figure 3a) and a ZP of -63.8 mV (Figure 3b). This negative ZP indicates high stability of SFSC-Ag-NPs, likely due to the presence of stabilizing agents that are absorbed onto their surface. These stabilizing agents create electrostatic repulsion between the Ag-NPs, which helps to minimize

aggregation [44-46]. The z-average size found in this study was generally smaller, and the ZP was more negative than in previous research [47, 48]. For instance, Ibrahim et al. [47] reported that Ag-NPs bio-synthesized with *Acacia raddiana* extract had a z-average size of approximately 77.35 nm and a ZP of -32.2 mV, while Maryani et al. [48] discovered that the Ag-NPs made using *Desmodium triquetrum* extract had an average z-size of 88.8 nm and a ZP of -27.4 mV.

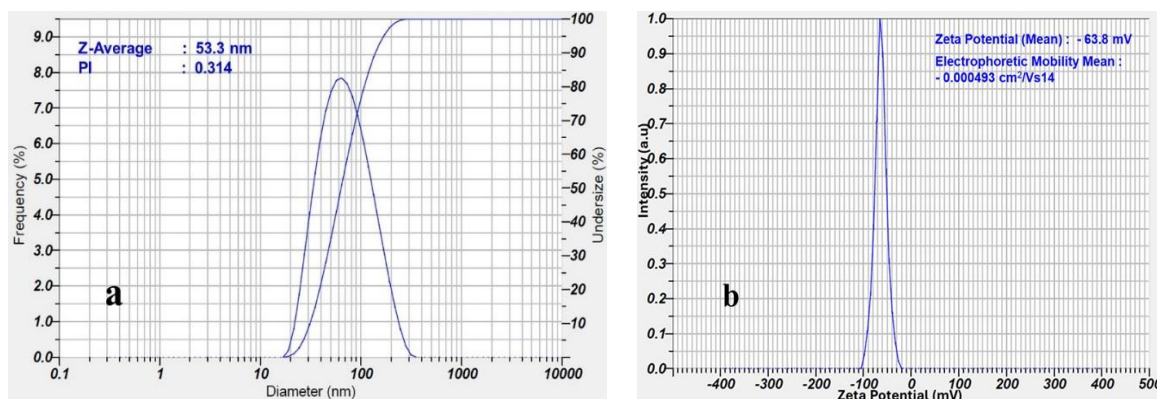


Figure 3. (a) DLS particle size distribution; (b) zeta potential of colloidal SFSC-Ag-NPs.

Fourier Transform Infrared Spectroscopy (FTIR) is an important technique in studying the interactions of biomolecules involved in the fabrication and stabilization of nanoparticles. Figure 4a shows the FTIR spectrum for SFSC water extracts (red line) and colloidal SFSC-Ag-NPs (blue line). Both spectra show prominent absorption bands in the 3100–3600 cm⁻¹ range, associated with the hydroxyl functional group's O–H stretch vibrations [21, 26]. Bands in the range of 2000–2400 cm⁻¹ relate to the stretching of C≡C bonds and C=O vibrations of alkyne and carbonyl groups [21, 30]. Peaks observed in the 1500–1750 cm⁻¹ range show C=C alkenyl stretching, primary amine N-H bending, and C=O stretching of amide [21]. The bands in the 800–1200 cm⁻¹ region are related to the stretching of C–O and C–N, characteristic of the alcohol and amine groups [23, 30]. Further, bands between 500–550 cm⁻¹ can be associated with metal-oxygen vibrations [22], which confirms the interaction between Ag⁰ and the functional group of biomolecules derived from SFSC extract. The data from this FTIR analysis indicated that the hydroxyl (OH), alkyne (C≡C), carbonyl (C=O), alkenyl (C=C), and amine (NH) groups in SFSC extract facilitated the reduction of Ag⁺ to Ag⁰ and its stabilization.

X-ray powder diffraction analysis is a widely utilized method for gathering information about a material's crystallinity, phase composition, and structural characteristics. Figure 4b displays the XRD pattern of SFSC-Ag-NPs, highlighting diffraction peaks at 2θ: 38.03°, 44.39°, 64.37°, and 77.30°. These peaks correspond to the (111), (200), (220), and (311) crystal planes of Ag⁰, which have a face-centered cubic structure (FCC) (JCPDS file no. 03-0921) [38, 49, 50]. The sharp intensity of these peaks indicates that the SFSC-Ag-NPs possess a well-defined crystal structure. The crystallite size of the SFSC-Ag-NPs is approximately 12.9 nm, determined using the Debye-Scherrer equation [51-53] based on the full width at half maximum (FWHM) values of the (111) peak. Additionally, two other peaks observed at 2θ: 28.42° and 47.14° are attributed to the (111) and (220) Si crystal planes (JCPDS file no. 27-1402) [54]. It's crucial to recognize that the quality of Si wafers significantly influences the crystallographic orientation of the detected Si peaks [38]. The XRD patterns observed in this study are consistent with previous research on the biofabrication of Ag-NPs using plant extracts. For instance, biofabricated Ag-NPs mediated by *Ocimum sanctum* leaf extract exhibited peaks at 2θ: 38.10°,

44.15°, 64.67°, and 77.54° [49]. Similarly, a study on the biofabrication of Ag-NPs using *Curcuma longa* extract reported diffraction peaks at 2θ : 38.18°, 44.25°, 64.72°, and 77.40° [52]. All diffraction peaks in both studies correspond to the (111), (200), (220), and (311) crystal planes of the FCC Ag⁰ structure.

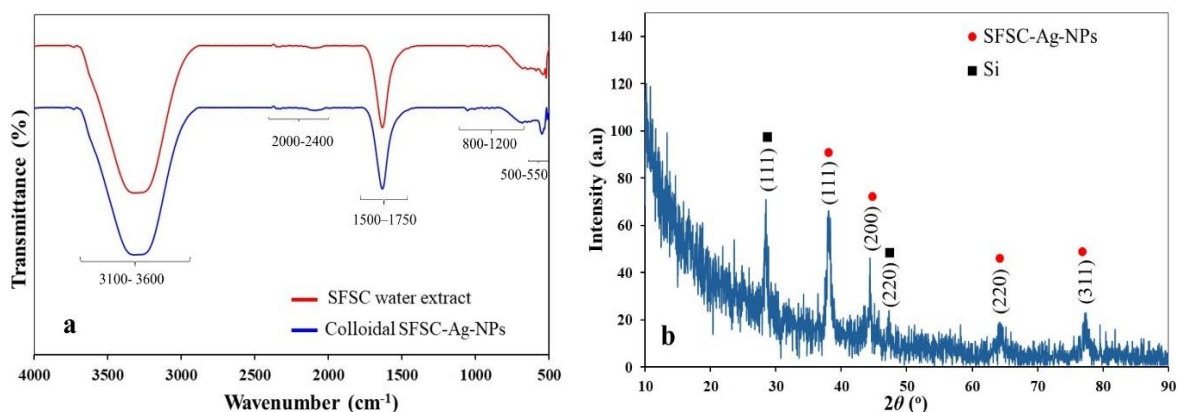


Figure 4. (a) FT-IR spectra of SFSC water extract and colloidal SFSC-Ag-NPs; (b) XRD pattern of SFSC-Ag-NPs applying a grazing incident angle 1°

Analytical data from a high-resolution transmission electron microscope can provide detailed information regarding a material's structural and morphological characteristics. Figure 5 is a representative HR-TEM SFSC-Ag-NPs micrograph. Figure 5 (a and b) confirms the shape of the SFSC-Ag-NPs particles, suggesting that most SFSC-Ag-NPs particles are quasi-spherical with a clear dispersion, although some of the particles are hexagonal. Other shapes of Ag-NPs, including spherical, rectangular, and triangular, have also been reported by previous studies [21, 55]. In addition, the image in Figure 5 (a and b) also shows some boundary layers surrounding the SFSC-Ag-NPs. The boundary layers might arise from bioactive constituents in the SFSC water extract, which act as a capping agent. Similar boundary layer formation has also been reported previously in biofabricated Ag-NPs using extracts of *D. celebica* [38], *Zizyphus spina-christi* [56], and *Parkia speciosa* [57]. The size distribution of SFSC-Ag-NPs (Figure 5c) indicates that the nanoparticles are less uniform, with a range of sizes between 10 and 20 nm and an average size of 14.42 nm. It is important to note that the SFSC-Ag-NPs particle sizes obtained from DLS analysis (Figure 3a) differ from the results of measurements using TEM (Figure 5c). This occurs because DLS measures the hydrated particle size in suspension, whereas TEM captures their physical dimensions in a dry state [58]. The small particle size of Ag-NPs found in this study is similar to the findings of Ibrahim et al. [47] and Rana et al. [45]. They reported biofabricated Ag-NPs with sizes ranging from 8-41 nm and 25-28 nm, respectively. The selected area electron diffraction (SAED) pattern (Figure 5d) features rings aligned for (111), (200), (220), and (311) of the FCC Ag⁰ 52 crystal planes. This finding is corroborated by the lattice fringe images of SFSC-Ag-NPs (Figures 5e and 5f), which show crystal structures with interplanar spacing of 0.235 nm and 0.204 nm, respectively, ascribing the (111) and (220) crystal planes.

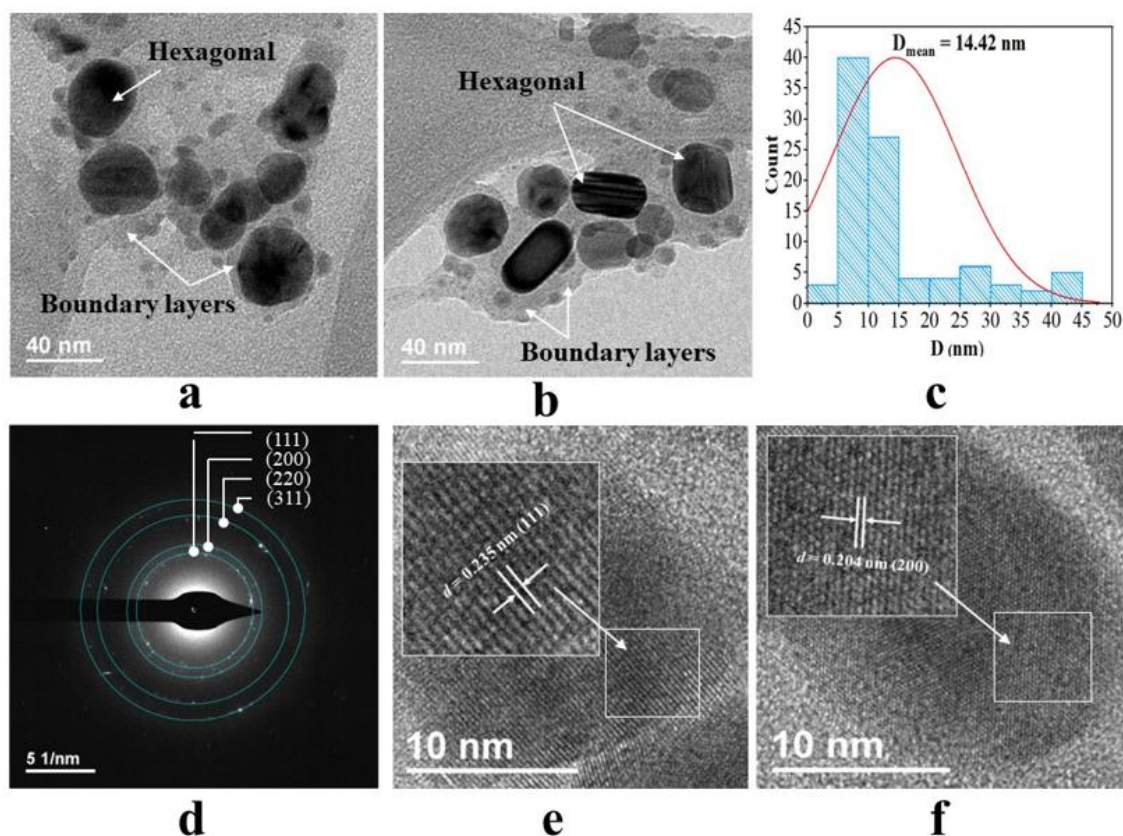


Figure 5. (a, b) representative HM-TEM images at 40 nm magnification with boundary layers; (c) particle size distribution with a mean diameter of 14.42 nm; (d) SAED; (e, f) lattice fringe of SFSC-Ag-NPs

3.2. Catalytic degradation of MB.

The efficiency of biofabricated Ag-NPs mediated by plant extracts as a catalyst in degrading dyes has attracted attention. Previous studies have shown that Ag-NPs successfully catalyze MB degradation [36, 59-61]. Figures 6a and 6b show the reaction time on the absorbance and efficiency of MB degradation. The results were obtained from an experiment conducted for 17 minutes at neutral pH, using a concentration of MB at 20 ppm and a volume of 3 ml. Meanwhile, the volumes of NaBH_4 and SFSC-Ag-NPs were 100 μL and 200 μL , respectively. Figure 6a presents two data sets, i.e., the blue square represents the absorbance (a.u.) over time, while the dotted red square represents the degradation efficiency. In the initial reaction stage, there is a slow decrease in absorbance (58.94% efficiency before 12 min). The reaction involves the gradual activation of the active site and the adsorption of MB to the surface of Ag-NPs. It is followed by a sharp decrease in absorbance after 12 minutes due to increased catalyst activity that accelerates the degradation reaction. The sharp drop after 12 minutes indicates an optimal catalytic performance, likely due to the full activation of Ag-NPs and increased interaction between MB and NaBH_4 . At 17 minutes, absorbance is close to zero (99.84% efficiency), which confirms that the degradation of MB is near complete [60]. These findings align with the fact that the UV-Vis absorbance spectrum of MB has decreased gradually over time (Figure 6b). The maximum absorbance observed at 0 minutes of reaction indicates that the methylene blue (MB) concentration has remained unchanged. Then, the absorbance decreases to near zero, accompanied by a visible color development from blue to yellowish (Figure 6b; insert). These findings imply that reaction time shows a vital role in the degradation process of MB using Ag-NPs, which impacts the degradation process's efficiency and completeness [59]. Adequate reaction time facilitates dye molecules' adsorption, diffusion,

and interaction with active sites on the catalyst surface [40, 53, 62, 63]. In contrast, insufficient reaction time may lead to incomplete degradation, while a long reaction time may not be necessary. Thus, optimizing reaction time is essential to achieve maximum degradation efficiency.

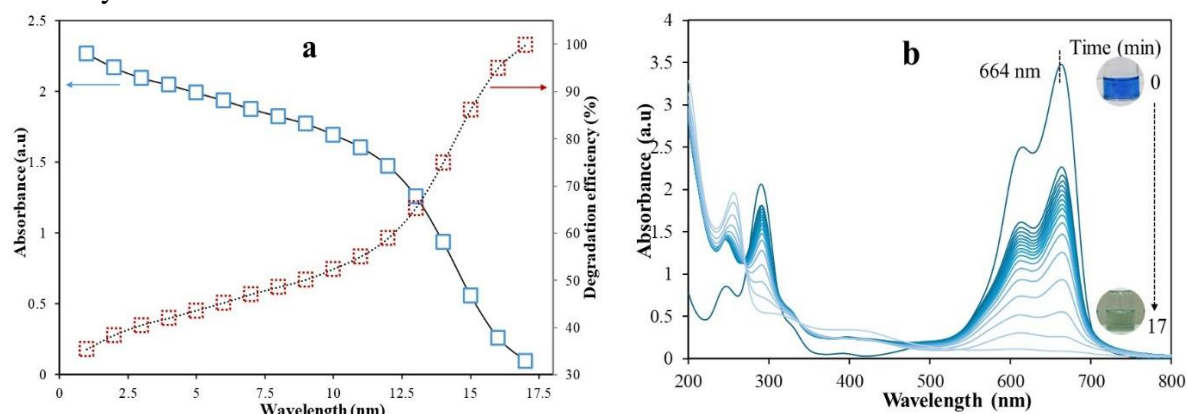


Figure 6. Effect of reaction time on (a) MB absorbance reduction during catalytic degradation by SFSC-Ag-NPs. Each blue square point represents the peak at 664 nm and the corresponding degradation efficiency (dotted red square); (b) the absorbance spectra of degraded MB.

Figure 7 shows the effect of the initial concentration of MB and the volume of SFSC-Ag-NPs on the change in absorbance of UV-Vis MB, obtained under experimental conditions with a volume of 3ml MB and 100 μL of NaBH_4 , a reaction time of 20 min, and a neutral pH. Figure 7a presents the impact of the initial concentration of MB on their UV-Vis absorbance spectrum. At low MB concentrations (<10 ppm), absorbance decreases faster than at high concentrations (>15 ppm). It indicates greater catalytic efficiency because, under these conditions, the dye molecules can easily access the active site of Ag-NPs. In contrast, at high MB concentrations, the degradation rate slows down due to the saturation of active sites of Ag-NPs, where this condition triggers competition among dye molecules [36]. Moreover, Figure 7b shows the relationship between SFSC-Ag-NPs volume and degradation efficiency. When the volume of SFSC-Ag-NPs increased from 100 μL to 200 μL , the absorbance of MB decreased significantly, and there was an increase in efficiency from 33.48% to nearly 100%. This drastic increase in efficiency can be caused by the higher catalyst volume, the more active sites for degradation reactions to occur [59]. However, beyond 200 μL , the degradation efficiency is plateaus, indicating the optimal catalyst volume and all MB molecules are effectively degraded.

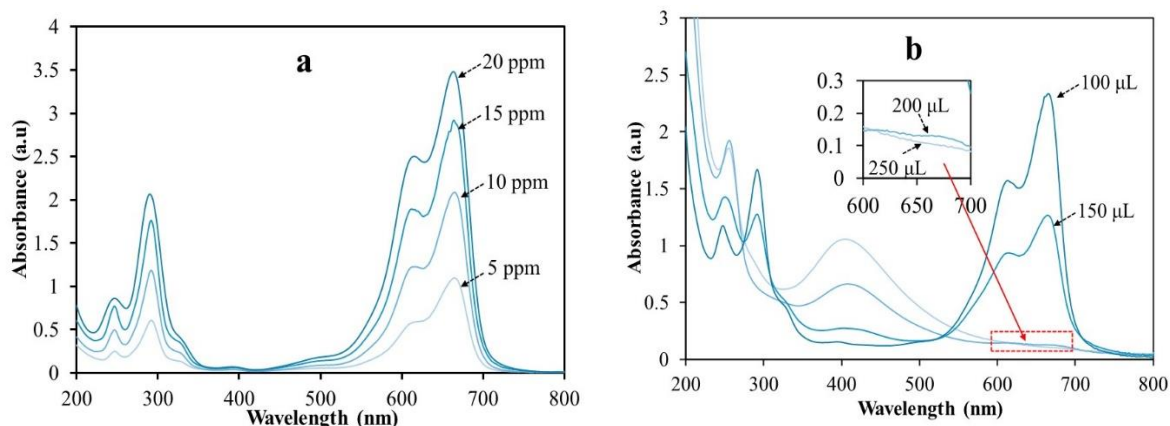


Figure 7. Effect of (a) initial MB concentration (ppm); (b) SFSC-Ag-NPs volume (μL) on the absorbance of MB.

Figure 8 presents the kinetic patterns of 1st-order (blue squares) and 2nd-order (black squares) models for MB degradation by SFSC-Ag-NPs. It illustrates changes in MB concentration over time and how well both models fit the data. Since NaBH₄ was present in large excess ([NaBH₄]:[MB] = 51.6), its concentration remained nearly constant throughout the reaction. Under these conditions, the reaction was expected to follow pseudo-order kinetics. Reaction rate constants and other kinetic parameters are listed in Table 1. Based on the evaluation of reaction kinetic parameters using both models, the rate constants for the pseudo-1st- and pseudo-2nd-orders were obtained at $9.47 \times 10^{-2} \text{ min}^{-1}$ (with $R^2 = 0.966$) and $1.12 \times 10^{-2} \text{ L mg}^{-1} \text{ min}^{-1}$ (with $R^2 = 0.853$), respectively. A higher regression correlation coefficient for the pseudo-1st-order ($R^2 = 0.966$) implies a better fit to the experimental data than the pseudo-2nd-order ($R^2 = 0.853$). Therefore, it is concluded that the catalytic degradation of MB by SFSC-Ag-NPs follows the kinetics of the pseudo-1st-order rate. These findings suggest that the reaction rate increases in direct proportion to the concentration of MB, offering a more precise depiction of the degradation process. The reaction rate observed in our study was significantly higher than previously reported [64, 65], demonstrating superior efficiency and faster MB removal by biofabricated SFSC-Ag-NPs.

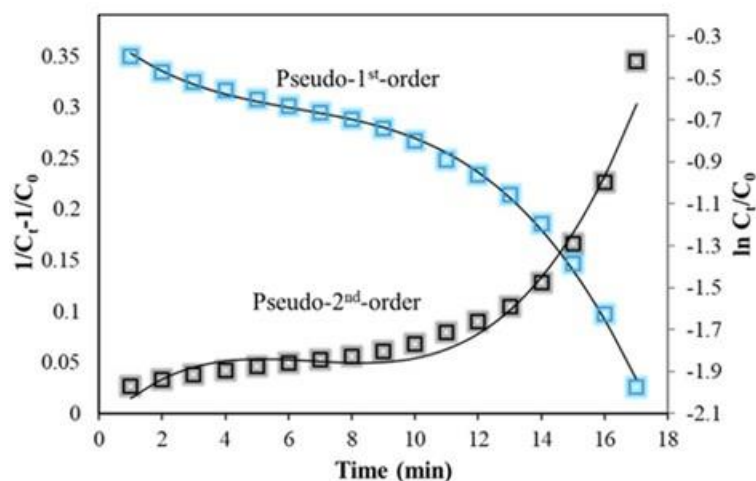


Figure 8. Pseudo-1st-order (blue square line) and pseudo-2nd-order (black square line) kinetics of catalytic degradation of MB by SFSC-Ag-NPs.

Table 1. Kinetic models for MB catalytic degradation by SFSC-Ag-NPs with NaBH₄.

Model of chemical kinetic	R ²	Rate constant	Rate constant (unit)
1 st -order	R ² = 0.966	9.47×10^{-2}	min ⁻¹
2 nd -order	R ² = 0.853	1.12×10^{-2}	L mg ⁻¹ min ⁻¹

The catalytic mechanism of MB degradation by Ag-NPs has been well proposed [38, 59, 60, 66, 67]. The high efficiency obtained from the SFSC-Ag-NPs catalyst most likely follows the same mechanism path, where SFSC-Ag-NPs play a role in accelerating electron transfer during MB reduction by NaBH₄. In this process, SFSC-Ag-NPs particles dominated by small size (see Figure 5c) have a larger surface area, thus increasing the number of active sites for electron transfer. This larger surface area allows for more efficient interactions between electron donors (NaBH₄) and electron acceptors (MB), ultimately accelerating the reduction reaction. In addition, the small size of SFSC-Ag-NPs increases the dispersion rate, shortens the electron transfer distance, and reduces kinetic resistance in catalytic reactions. Thus, the small size of SFSC-Ag-NPs, which is strongly presumed, plays a significant role in enhancing the catalytic efficiency of MB reduction by NaBH₄.

4. Conclusions

In conclusion, SFSC-Ag-NPs were successfully synthesized from AgNO₃ using a water extract from the seed coat of *S. foetida* (SFSC) through a green approach. Functional groups such as hydroxyl (OH), alkyne (C≡C), carbonyl (C=O), alkenyl (C=C), and amine (NH) in SFSC water extract are accountable for the reduction and stabilization. Characterization confirms that Ag-NPs have quasi-spherical and hexagonal shapes, the average particle size measures 14.42 nm, and good crystalline properties. The catalytic degradation of MB dye (20 ppm) by Ag-NPs with NaBH₄ as a reducing agent at neutral pH achieved an outstanding efficiency of 99.84% within 17 minutes. Kinetic studies revealed reactions following the pseudo-1st-order ($R^2 = 0.966$). The mechanism suggests that SFSC-Ag-NPs aid the transfer of electrons from H⁻ to MB, reducing oxidized MB (●MB) to its colorless, leuco-methylene blue (LMB) form. These findings highlight the outstanding catalytic efficiency of SFSC-Ag-NPs textile dye removal, highlighting their applicability for wastewater treatment and large-scale industrial applications.

Author Contributions

Conceptualization, Resources, Project Administration, Supervision, Methodology, Writing – original draft and editing, O.Z.; Data Curation, Formal Analysis, Validation, Investigation, F.A.D.; Validation, Formal Analysis, Supervision, Writing – review and editing, T.S. Each author has made a significant contribution according to their respective roles and has approved the final version of the manuscript for publication.

Institutional Review Board Statement

Not applicable.

Informed Consent Statement

Not applicable.

Data Availability Statement

Data supporting the findings of this study are available upon reasonable request from the corresponding author.

Funding

This research received no external funding.

Acknowledgments

The authors thank the instrument operators at ELSA-BRIN for their valuable aid in sample characterization. Additionally, they are grateful to the Chemistry Research Centre-BRIN for providing access to laboratory facilities, which was crucial in completing this study.

Conflicts of Interest

All authors affirm that no financial, personal, or professional conflicts of interest could have influenced the research findings, their analysis, or the conclusions presented in this study.

References

1. Shreyash, N.; Bajpai, S.; Khan, M.A.; Vijay, Y.; Tiwary, S.K.; Sonker, M. Green Synthesis of Nanoparticles and Their Biomedical Applications: A Review. *ACS Appl. Nano Mater.* **2021**, *4*, 11428–11457, <https://doi.org/10.1021/acsanm.1c02946>.
2. Nande, A.; Raut, S.; Michalska-Domanska, M.; Dhoble, S.J. Green Synthesis of Nanomaterials Using Plant Extract: A Review. *Curr. Pharm. Biotechnol.* **2021**, *22*, 1794–1811, <https://doi.org/10.2174/1389201021666201117121452>.
3. Moges, W.; Misskire, Y. Green synthesis, characterization and antibacterial activities of silver nanoparticles using *Sida schimperiana Hochst. ex A. Rich* (Chifrig) leaves extract. *Discov. Mater.* **2025**, *5*, 34, <https://doi.org/10.1007/s43939-025-00221-x>.
4. Harine, A.; Ranjani, S.; Hemalatha, S. Antifungal efficacy of Citrusfusion-mediated silver nanoparticles in *Candida* species. *BMC Biotechnol.* **2025**, *25*, 18, <https://doi.org/10.1186/s12896-025-00952-y>.
5. Ali, S.; Ijaz, H.; Ahmad, M.U.; Rukhma; Ullah, N.; Sarwar, A.; Khan, M.J.; Aziz, T.; shami, A.; Al-Asmari, F. Photocatalytic removal of textile wastewater-originated methylene blue and malachite green dyes using spent black tea extract-coated silver nanoparticles. *Sci. Rep.* **2025**, *15*, 1851, <https://doi.org/10.1038/s41598-025-85894-3>.
6. Abbigeri, M.B.; Thokchom, B.; Singh, S.R.; Bhavi, S.M.; Harini, B.P.; Yarajarla, R.B. Antioxidant and anti-diabetic potential of the green synthesized silver nanoparticles using *Martynia annua L.* root extract. *Nano TransMed* **2025**, *4*, 100070, <https://doi.org/10.1016/j.ntm.2025.100070>.
7. Gangal, A.; Choudhary, K.; Duseja, M.; Shukla, R.K.; Kumar, S. Green synthesis of Silver nanoparticles from plant oil for enzyme-functionalized optical fiber biosensor: Improved sensitivity and selectivity in ascorbic acid detection. *Opt. Laser Technol.* **2025**, *186*, 112635, <https://doi.org/10.1016/j.optlastec.2025.112635>.
8. Khatoon, U.T.; Velidandi, A.; Nageswara Rao, G.V.S. Sodium borohydride mediated synthesis of nano-sized silver particles: Their characterization, antimicrobial and cytotoxicity studies. *Mater. Chem. Phys.* **2023**, *294*, 126997, <https://doi.org/10.1016/j.matchemphys.2022.126997>.
9. Mavani, K.R.; Shah, M. Synthesis of Silver Nanoparticles by using Sodium Borohydride as a Reducing Agent. *Int. J. Eng. Res. Technol.* **2013**, *2*, 1-5, <http://dx.doi.org/10.13140/2.1.3116.8648>.
10. Gurusamy, V.; Krishnamoorthy, R.; Gopal, B.; Veeraravagan, V.; Neelamegam, P. Systematic investigation on hydrazine hydrate assisted reduction of silver nanoparticles and its antibacterial properties. *Inorg. Nano-Met. Chem.* **2017**, *47*, 761-767, <https://doi.org/10.1080/15533174.2015.1137074>.
11. Dugandžić, V.; Hidi, I.J.; Weber, K.; Cialla-May, D.; Popp, J. *In situ* hydrazine reduced silver colloid synthesis – Enhancing SERS reproducibility. *Anal. Chim. Acta* **2016**, *946*, 73–79, <https://doi.org/10.1016/j.aca.2016.10.018>.
12. Ahmed, S.; Ahmad, M.; Swami, B.L.; Ikram, S. A review on plants extract mediated synthesis of silver nanoparticles for antimicrobial applications: A green expertise. *J. Adv. Res.* **2016**, *7*, 17–28, <https://doi.org/10.1016/j.jare.2015.02.007>.
13. Vanlalveni, C.; Lallianrawna, S.; Biswas, A.; Selvaraj, M.; Changmai, B.; Rokhum, S.L. Green synthesis of silver nanoparticles using plant extracts and their antimicrobial activities: a review of recent literature. *RSC Adv.* **2021**, *11*, 2804-2837, <https://doi.org/10.1039/D0RA09941D>.
14. Mashwani, Z.-u.-R.; Khan, T.; Khan, M.A.; Nadhman, A. Synthesis in plants and plant extracts of silver nanoparticles with potent antimicrobial properties: current status and future prospects. *Appl. Microbiol. Biotechnol.* **2015**, *99*, 9923–9934, <https://doi.org/10.1007/s00253-015-6987-1>.
15. Chandraker, S.K.; Ghosh, M.K.; Lal, M.; Shukla, R. A review on plant-mediated synthesis of silver nanoparticles, their characterization and applications. *Nano Ex.* **2021**, *2*, 022008, <https://doi.org/10.1088/2632-959X/ac0355>.
16. Asimuddin, M.; Shaik, M.R.; Adil, S.F.; Siddiqui, M.R.H.; Alwarthan, A.; Jamil, K.; Khan, M. *Azadirachta indica* based biosynthesis of silver nanoparticles and evaluation of their antibacterial and cytotoxic effects. *J. King Saud Univ. Sci.* **2020**, *32*, 648–656, <https://doi.org/10.1016/j.jksus.2018.09.014>.

17. Singhal, M.; Loveleen, L.; Manchanda, R.; Syed, A.; Bahkali, A.H.; Wong, L.S.; Nimesh, S.; Gupta, N. Design, synthesis and optimization of silver nanoparticles using *Azadirachta indica* bark extract and its antibacterial application. *J. Agric. Food Res.* **2024**, *16*, 101088, <https://doi.org/10.1016/j.jafr.2024.101088>.
18. Haris, Z.; Ahmad, I. Green synthesis of silver nanoparticles using *Moringa oleifera* and its efficacy against gram-negative bacteria targeting quorum sensing and biofilms. *J. Umm Al-Qura Univ. Appl. Sci.* **2024**, *10*, 156–167, <https://doi.org/10.1007/s43994-023-00089-8>.
19. Younas, M.; Rasool, M.H.; Khurshid, M.; Khan, A.; Nawaz, M.Z.; Ahmad, I.; Lakhan, M.N. *Moringa oleifera* leaf extract mediated green synthesis of silver nanoparticles and their antibacterial effect against selected gram-negative strains. *Biochem. Syst. Ecol.* **2023**, *107*, 104605, <https://doi.org/10.1016/j.bse.2023.104605>.
20. Tran Khac, K.; Hoang Phu, H.; Tran Thi, H.; Dinh Thuy, V.; Do Thi, H. Biosynthesis of silver nanoparticles using tea leaf extract (*Camellia sinensis*) for photocatalyst and antibacterial effect. *Heliyon* **2023**, *9*, e20707, <https://doi.org/10.1016/j.heliyon.2023.e20707>.
21. Farsana, S.; Ansil, P.N.; Sumalekshmy, S.; Soumya, S. Biogenic synthesis of silver nanoparticles using *Sterculia foetida* seed extract and evaluation of its therapeutic potential. *Mater. Today: Proc.* **2023**, <https://doi.org/10.1016/j.matpr.2023.11.080>.
22. Jana, K.; Ghosh, S.; Ghosh, A.; Parua, P.; Samanta, S.; Das, S.; Debnath, B. Silver Nanoparticles Loaded with Bark Extract of *Sterculia foetida*: Their Green Synthesis, Characterization, and Anti-bacterial Activity Evaluation. *Bionatura J.* **2024**, *1*, 1–19, <https://doi.org/10.70099/BJ/2024.01.03.17>.
23. Teli, M.D.; Pandit, P. Application of *Sterculia foetida* Fruit Shell Waste Biomolecules on Silk for Aesthetic and Wellness Properties. *Fibers Polym.* **2018**, *19*, 41–54, <https://doi.org/10.1007/s12221-018-7315-4>.
24. Lim, T.K. *Sterculia foetida*. In *Edible Medicinal And Non Medicinal Plants: Volume 3, Fruits*, Lim, T.K., Ed.; Springer Netherlands: Dordrecht, **2012**; pp. 192-197, https://doi.org/10.1007/978-94-007-2534-8_26.
25. Jafri, A.; Shabana, B.; Juhi, R.; Fahad, K.; Neelam, S.; K., S.A.; and Arshad, M. Phytochemical screening of *Sterculia foetida* seed extract for anti-oxidant, antimicrobial activity, and detection of apoptosis through reactive oxygen species (ROS) generation, mitochondrial membrane potential (MMP) decrease, and nuclear fragmentation in human osteosarcoma cells. *Journal of Histotechnology* **2019**, *42*, 68-79, <https://doi.org/10.1080/01478885.2019.1592832>.
26. Jana, K.; Ghosh, A.; Debnath, B.; Das, S. GC-MS Analysis of Phytocomponents of Methanolic Bark Extract of *Sterculia foetida*. *Res. J. Pharm. Technol.* **2023**, *16*, 5624-5630, <https://doi.org/10.52711/0974-360X.2023.00909>.
27. Tuyen, P.N.K.; Trang, N.T.Q.; Doan, H.C.; Thuong, P.D.; Duan, N.T.; Cuong, T.D.D.; Chi, H.B.L.; Tuyet, N.T.A.; Phung, N.K.P.; Nguyen, T.T.-H. Triterpenoids and coumarins from the leaves of *Sterculia foetida* Linn. *J. Sci. Technol. Develop.* **2020**, *23*, 763–768, <https://doi.org/10.32508/stdj.v23i4.2449>.
28. Cuong, D.T.D.; Dat, H.T.; Duan, N.T.; Thuong, P.D.; Phat, N.T.; Tri, M.D.; Van Son, D.; Hoa, N.T.; Tuyen, P.N.K.; Phung, N.K.P. Isolation and characterization of six flavonoids from the leaves of *Sterculia foetida* Linn.. *VJCH.* **2019**, *57*, 438-442. <https://doi.org/10.1002/vjch.201900084>.
29. Rajasekharreddy, P.; Rani, P.U. Biofabrication of Ag nanoparticles using *Sterculia foetida* L. seed extract and their toxic potential against mosquito vectors and HeLa cancer cells. *Mater. Sci. Eng. C* **2014**, *39*, 203–212, <https://doi.org/10.1016/j.msec.2014.03.003>.
30. Kudle, K.R.; Donda, M.R.; Merugu, R.; Prashanthi, Y.; Kudle, M.R.; Pratap, R.M.P. Green synthesis of silver nanoparticles using water-soluble gum of *Sterculia foetida* and evaluation of its antimicrobial activity. *Int. J. Res. Pharm. Sci.* **2013**, *4*, 563–568.
31. Pandit, P.; Teli, M.D.; Nadathur, G.T.; Maiti, S.; Singha, K.; Maity, S. Green synthesis of nanoparticle and its application on cotton fabric using *Sterculia foetida* fruit shell extract. *J. Text. Eng. Fash. Technol.* **2020**, *6*, 257–265, <https://doi.org/10.15406/jteft.2020.06.00259>.
32. Ganapuram, B.R.; Alle, M.; Dadigala, R.; Dasari, A.; Maragoni, V.; Guttena, V. Catalytic reduction of methylene blue and Congo red dyes using green synthesized gold nanoparticles capped by *salmlalia malabarica* gum. *Int. Nano Lett.* **2015**, *5*, 215–222, <https://doi.org/10.1007/s40089-015-0158-3>.
33. Khan, I.; Saeed, K.; Zekker, I.; Zhang, B.; Hendi, A.H.; Ahmad, A.; Ahmad, S.; Zada, N.; Ahmad, H.; Shah, L.A.; Shah, T.; Khan, I. *Review on Methylene Blue: Its Properties, Uses, Toxicity and Photodegradation.* *Water* **2022**, *14*, 242, <https://doi.org/10.3390/w14020242>.
34. Taldiev, A.; Terekhov, R.; Nikitin, I.; Melnik, E.; Kuzina, V.; Klochko, M.; Reshetov, I.; Shiryaev, A.; Loschenov, V.; Ramenskaya, G. Methylene blue in anticancer photodynamic therapy: systematic review of preclinical studies. *Front. Pharmacol.* **2023**, *14*, 1264961, <https://doi.org/10.3389/fphar.2023.1264961>.

35. Oladoye, P.O.; Ajiboye, T.O.; Omotola, E.O.; Oyewola, O.J. Methylene blue dye: Toxicity and potential elimination technology from wastewater. *Results Eng.* **2022**, *16*, 100678, <https://doi.org/10.1016/j.rineng.2022.100678>.
36. Ogundare, S.A.; Adesetan, T.O.; Muungani, G.; Moodley, V.; Amaku, J.F.; Atewolara-Odule, O.C.; Yussuf, S.T.; Sanyaolu, N.O.; Ibikunle, A.A.; Balogun, M.S.; Ewald van Zyl, W. Catalytic degradation of methylene blue dye and antibacterial activity of biosynthesized silver nanoparticles using *Peltophorum pterocarpum* (DC.) leaves. *Environ. Sci. Adv.* **2023**, *2*, 247–256, <https://doi.org/10.1039/D2VA00164K>.
37. Sahin, M.; Gubbuk, I.H. Green synthesis of palladium nanoparticles and investigation of their catalytic activity for methylene blue, methyl orange and rhodamine B degradation by sodium borohydride. *React. Kinet. Mech. Catal.* **2022**, *135*, 999–1010, <https://doi.org/10.1007/s11144-022-02185-y>.
38. Zuas, O.; Ariani, N.; Devy, Y.A.; Sudiro, T. Biosynthesis and Characterization of Silver Nanoparticles Mediated by Seed Extract of Macassar Ebony with Catalytic and Antimicrobial Activity. *J. Inorg. Organomet. Polym. Mater.* **2025**, *35*, 1563-1573, <https://doi.org/10.1007/s10904-024-03384-x>.
39. Gangwar, J.; Joseph, K.S. Eco-conscious photocatalytic degradation of organic textile dyes using green synthesized silver nanoparticles: a safe and green approach toward sustainability. *Biomass Convers. Biorefin.* **2024**, <https://doi.org/10.1007/s13399-024-05348-0>.
40. Ahmad, A.; Roy, P.G.; Hassan, A.; Zhou, S.; Azam, M.; Sial, M.A.Z.G.; Irfan, A.; Kanwal, F.; Begum, R.; Farooqi, Z.H. Catalytic degradation of various dyes using silver nanoparticles fabricated within chitosan based microgels. *Int. J. Biol. Macromol.* **2024**, *283*, 137965, <https://doi.org/10.1016/j.ijbiomac.2024.137965>.
41. Golmohammadi, M.; Hassankiadeh, M.N.; AlHammadi, A.; Elkamel, A. Fabrication of Green Synthesized SnO₂-ZnO/Bentonite Nanocomposite for Photocatalytic Degradation of Organic Dyes. *J. Clust. Sci.* **2023**, *34*, 2275–2286, <https://doi.org/10.1007/s10876-022-02379-3>.
42. Mukadam, M.; Khan, N.A.M.; Khan, S.; Kauchali, A. UV-Vis Spectroscopy in Analysis of Phytochemicals. *Int. J. Pharm. Res. Appl.* **2021**, *6*, 482–499.
43. Farkas, N.; Kramar, J.A. Dynamic light scattering distributions by any means. *J. Nanopart. Res.* **2021**, *23*, 120, <https://doi.org/10.1007/s11051-021-05220-6>.
44. Sezer, N.; Atieh, M.A.; Koç, M. A comprehensive review on synthesis, stability, thermophysical properties, and characterization of nanofluids. *Powder Technol.* **2019**, *344*, 404–431, <https://doi.org/10.1016/j.powtec.2018.12.016>.
45. Rana, N.; Banu, A.N.; Kumar, B.; Singh, S.K.; Abdel-razik, N.E.; Jalal, N.A.; Bantun, F.; Vamanu, E.; Singh, M.P. Phytofabrication, characterization of silver nanoparticles using Hippophae rhamnoides berries extract and their biological activities. *Front. Microbiol.* **2024**, *15*, 1399937, <https://doi.org/10.3389/fmicb.2024.1399937>.
46. Bélteky, P.; Rónavári, A.; Igaz, N.; Szerencsés, B.; Tóth, I.Y.; Pfeiffer, I.; Kiricsi, M.; Kónya, Z. Silver nanoparticles: aggregation behavior in biorelevant conditions and its impact on biological activity. *Int. J. Nanomed.* **2019**, *14*, 667–687, <https://doi.org/10.2147/IJN.S185965>.
47. Ibrahim, N.H.; Taha, G.M.; Hagaggi, N.S.A.; Moghazy, M.A. Green synthesis of silver nanoparticles and its environmental sensor ability to some heavy metals. *BMC Chem.* **2024**, *18*, 7, <https://doi.org/10.1186/s13065-023-01105-y>.
48. Maryani, F.; Septama, A.W. Microwave-assisted green synthesis of *Desmodium triquetrum*-mediated silver nanoparticles: enhanced antibacterial, antibiofilm, and cytotoxicity activities against human breast cancer cell lines. *Mater. Adv.* **2022**, *3*, 8267–8275, <https://doi.org/10.1039/d2ma00613h>.
49. Singhal, G.; Bhavesh, R.; Kasariya, K.; Sharma, A.R.; Singh, R.P. Biosynthesis of silver nanoparticles using *Ocimum sanctum* (Tulsi) leaf extract and screening its antimicrobial activity. *J. Nanopart. Res.* **2011**, *13*, 2981–2988, <https://doi.org/10.1007/s11051-010-0193-y>.
50. Kumar, S.V.; Bafana, A.P.; Pawar, P.; Rahman, A.; Dahoumane, S.A.; Jeffryes, C.S. High conversion synthesis of <10 nm starch-stabilized silver nanoparticles using microwave technology. *Sci. Rep.* **2018**, *8*, 5106, <https://doi.org/10.1038/s41598-018-23480-6>.
51. Ashokkumar, M.; Palanisamy, K.; Ganesh Kumar, A.; Muthusamy, C.; Senthil Kumar, K.J. Green synthesis of silver and copper nanoparticles and their composites using *Ocimum sanctum* leaf extract displayed enhanced antibacterial, antioxidant and anticancer potentials. *Artif. Cells Nanomed. Biotechnol.* **2024**, *52*, 438-448, <https://doi.org/10.1080/21691401.2024.2399938>.
52. Shameli, K.; Ahmad, M.B.; Shabanzadeh, P.; Jaffar Al-Mulla, E.A.; Zamanian, A.; Abdollahi, Y.; Jazayeri, S.D.; Eili, M.; Jalilian, F.A.; Haroun, R.Z. Effect of Curcuma longa tuber powder extract on size of silver

- nanoparticles prepared by green method. *Res. Chem. Intermed.* **2014**, *40*, 1313-1325, <https://doi.org/10.1007/s11164-013-1040-4>.
53. Zuas, O.; Budiman, H. Synthesis of Nanostructured Copper-doped Titania and Its Properties. *Nano-Micro Lett.* **2013**, *5*, 26-33, <https://doi.org/10.1007/BF03353728>.
 54. Yi, Z.; Lin, N.; Xu, T.; Qian, Y. TiO₂-coated Si/C interconnected microsphere with stable framework and interface for high-rate lithium storage. *Chem. Eng. J.* **2018**, *347*, 214-222, <https://doi.org/10.1016/j.cej.2018.04.101>.
 55. Shaban, S.M.; Aiad, I.; El-Sukkary, M.M.; Soliman, E.A.; El-Awady, M.Y. One-step green synthesis of hexagonal silver nanoparticles and their biological activity. *J. Ind. Eng. Chem.* **2014**, *20*, 4473-4481, <https://doi.org/10.1016/j.jiec.2014.02.019>.
 56. Halawani, E.M. Rapid Biosynthesis Method and Characterization of Silver Nanoparticles Using *Zizyphus spina christi* Leaf Extract and Their Antibacterial Efficacy in Therapeutic Application. *J. Biomater. Nanobiotechnol.* **2017**, *8*, 22-35, <https://doi.org/10.4236/jbnb.2017.81002>.
 57. Yusof, K.N.; Alias, S.S.; Harun, Z.; Basri, H.; Azhar, F.H. *Parkia speciosa* as Reduction Agent in Green Synthesis Silver Nanoparticles. *ChemistrySelect* **2018**, *3*, 8881-8885, <https://doi.org/10.1002/slct.201801846>.
 58. Stetefeld, J.; McKenna, S.A.; Patel, T.R. Dynamic light scattering: a practical guide and applications in biomedical sciences. *Biophys. Rev.* **2016**, *8*, 409-427, <https://doi.org/10.1007/s12551-016-0218-6>.
 59. Ullah, R.; Yaqub, A.; Ditta, S.A.; Tanvir, F.; Bilal, M.; Ali, S.; Anjum, K.M. Synthesis of silver nanoparticles and their use in the degradation of methylene blue dye and evaluation of in vitro antioxidant activity: a step toward sustainability. *Int. J. Environ. Sci. Technol.* **2025**, *22*, 2673-2682, <https://doi.org/10.1007/s13762-024-05782-7>.
 60. Kahraman, H.T. Synthesis of silver nanoparticles using *Alchemilla vulgaris* and *Helichrysum arenarium* for methylene blue and 4-nitrophenol degradation and antibacterial applications. *Biomass Convers. Biorefin.* **2024**, *14*, 13479-13490, <https://doi.org/10.1007/s13399-024-05314-w>.
 61. Sharma, A.; Sunny, S.; Arulraj, J.; Hegde, G. Exploring the efficiency of green synthesized silver nanoparticles as photocatalysts for organic dye degradation: unveiling key insights. *Nano Ex.* **2024**, *5*, 022002, <https://doi.org/10.1088/2632-959X/ad4d09>.
 62. Jara, Y.S.; Mekiso, T.T.; Washe, A.P. Highly efficient catalytic degradation of organic dyes using iron nanoparticles synthesized with *Vernonia Amygdalina* leaf extract. *Sci. Rep.* **2024**, *14*, 6997, <https://doi.org/10.1038/s41598-024-57554-5>.
 63. Javaid, R.; Qazi, U.Y. Catalytic Oxidation Process for the Degradation of Synthetic Dyes: An Overview. *Int. J. Environ. Res. Public Health* **2019**, *16*, 2066, <https://doi.org/10.3390/ijerph16112066>.
 64. Bogireddy, N.K.R.; Kiran Kumar, H.A.; Mandal, B.K. Biofabricated silver nanoparticles as green catalyst in the degradation of different textile dyes. *J. Environ. Chem. Eng.* **2016**, *4*, 56-64, <https://doi.org/10.1016/j.jece.2015.11.004>.
 65. Chikkanayakanahalli Paramesh, C.; Halligudra, G.; Gangaraju, V.; Sriramoju, J.B.; Shastri, M.; Kachigere B, H.; Habbanakuppe D, P.; Rangappa, D.; Kanchugarakoppal Subbegowda, R.; Doddakunche Shivaramu, P. Silver nanoparticles synthesized using saponin extract of *Simarouba glauca* oil seed meal as effective, recoverable and reusable catalyst for reduction of organic dyes. *Results Surf. Interfaces* **2021**, *3*, 100005, <https://doi.org/10.1016/j.rsurfi.2021.100005>.
 66. Hu, M.; Yan, X.; Hu, X.; Feng, R.; Zhou, M. Synthesis of silver decorated silica nanoparticles with rough surfaces as adsorbent and catalyst for methylene blue removal. *J. Sol-Gel Sci. Technol.* **2019**, *89*, 754-763, <https://doi.org/10.1007/s10971-018-4871-z>.
 67. Zahid, M.; Segar, A.S.M.; Al-Majmaie, S.; Shather, A.H.; Khan, M.F.; Alguno, A.C.; Capangpangan, R.Y.; Ismail, A. *Elettaria cardamomum* seed extract synthesized silver nanoparticles for efficient catalytic reduction of toxic dyes. *Environ. Nanotechnol. Monit. Manag.* **2023**, *20*, 100809, <https://doi.org/10.1016/j.enmm.2023.100809>.

Publisher's Note & Disclaimer

The statements, opinions, and data presented in this publication are solely those of the individual author(s) and contributor(s) and do not necessarily reflect the views of the publisher and/or the editor(s). The publisher and/or the editor(s) disclaim any responsibility for the accuracy, completeness, or reliability of the content. Neither the publisher nor the editor(s) assume any legal liability for any errors, omissions, or consequences arising from the

use of the information presented in this publication. Furthermore, the publisher and/or the editor(s) disclaim any liability for any injury, damage, or loss to persons or property that may result from the use of any ideas, methods, instructions, or products mentioned in the content. Readers are encouraged to independently verify any information before relying on it, and the publisher assumes no responsibility for any consequences arising from the use of materials contained in this publication.